Journal of Mining and Metallurgy, 39 (1–2) B (2003) 43 - 58.

ELECTROREFINING OF ALUMINUM ALLOY IN IONIC LIQUIDS AT LOW TEMPERATURES

V. Kamavaram[*], D. Mantha[**] and R.G. Reddy[***]

[*]*Graduate Student,* [**]*Research Associate and* [***]*ACIPCO Professor,*
Department of Metallurgical and Materials Engineering
[***]*Associate Director,* Center for Green Manufacturing
The University of Alabama, Tuscaloosa, AL-35487, USA

(Received 3 February 2003; accepted 22 April 2003)

Abstract

The electrorefining of aluminum alloy (A360) in ionic liquids at low temperatures has been investigated. The ionic liquid electrolyte was prepared by mixing anhydrous $AlCl_3$ and 1-Butyl-3-methylimidazolium chloride (BMIC) in appropriate proportions. The effect of the cell voltage, temperature, and the composition of the electrolyte on the electrorefining process has been studied. The characterization of the deposited aluminum was performed using scanning electron microscopy (SEM) and X-ray diffraction (XRD) techniques. The influence of experimental parameters such as cell voltage and concentration of $AlCl_3$ in the electrolyte on the deposit morphology was discussed. The composition of the aluminum deposits was analyzed using X-ray fluorescence spectrometer (XRF). Aluminum deposits with purity higher than 99.89 % were obtained. At a cell voltage of 1.0 V vs. Al/Al(III), the energy consumption was about 3 kWh/kg–Al. The main advantage of the process is low energy consumption compared to the existing industrial aluminum refining process.

Keywords: electrorefining, ionic liquids, aluminium alloy

1. Introduction

Aluminum is the second most commonly used metal in structural and automotive

applications [1]. There is an increasing demand for high purity aluminum mainly due to the growth of the electronic industry [2]. Pure aluminum is widely used in semiconductor processing, food service equipment, packaging equipment and life science/medical equipment. Excellent corrosion resistance properties make it a candidate material for coating metals that are intended for corrosive environments. Aluminum has been primarily produced by the ancient Hall-Héroult's electrolytic process since 1886 when it was discovered. The purity of aluminum produced by this process ranges from 99.5 to 99.9 %, therefore an additional refining process is required to produce high purity aluminum of >99.99 % purity level.

However, there are two methods currently in use for the production of high purity aluminum viz., three-layer electrolytic process and the segregation process. High temperatures (700–900 °C) and an energy consumption of 17–18 kWh/kg, which is higher than that for primary production, makes the three-layer electrolytic process economical only for high purity metal production [3]. The segregation process is a less energy consuming process compared to the three-layer one but the purity of aluminum produced is usually not higher than 99.98–99.99 % and sometimes additional refining steps are required in order to achieve high purity levels [3].

In 1854 Bunsen [4] developed the first non-aqueous electrolyte bath composed of fused $AlCl_3$–$NaCl$ for aluminum electrodeposition at low temperatures. Since then many molten salt electrolytic baths have been developed for depositing aluminum. In 1914 the first ionic liquid [$EtNH_3$-NO_3] was prepared. The most successful low temperature fused salt bath consisting of $AlBr_3$–tetraethyl ammonium bromide was developed by Keyes and Swann [5]. These low melting organic salt mixtures are called ionic liquids. Typically, these low melting ionic liquids represent a system, which is quite different from molten salts. Molten salt systems have a high melting point; they are highly viscous and very corrosive, whereas, ionic liquids have relatively low viscosity. Most of the ionic liquids are in the liquid state at room temperature and they are entirely composed of ions [6]. Large liquidus temperature range, negligible volatility, wide electrochemical window, and high thermal and electrical conductivities are the most important properties, which render ionic liquids to be potential solvents for electrochemical applications.

Later Hurley and Wier [7, 8] patented a fused salt bath, which consists of quaternary ammonium compound, ethylpyridinium bromide and $AlCl_3$ electrolytic composition. Electrolytes such as $AlBr_3$–alkyl benzene [9] and $AlBr_3$–KBr–benzene [10] were also used to electrodeposit aluminum but their low electrochemical window and low conductivity inhibited their development as electrolytic baths for aluminum electrodeposition. Welch and Osteryoung [11] later used $NaCl$–$AlCl_3$ at 175 °C and $AlCl_3$-butylpyridinum chloride at 30 °C to electrodeposit aluminum.

Wilkes et al. [12] developed a new class of low melting salts by combining $AlCl_3$ with 1-Methyl-3-ethylimidazolium chloride (*MEIC*). These melts have a wide electrochemi-

cal window and a large liquidus temperature range. The electrodeposition of aluminum in *MEIC–$AlCl_3$* [13] and *MEIC–$AlCl_3$*–benzene [14] electrolytic mixtures was reported. Thin deposits (<0.2 μm) in the former electrolyte and low conductivity of the electrolyte requiring the addition of co-solvents in the latter case made these mixtures unsuitable as electrolytes for aluminum electrodeposition. Recently [15, 16], we have found that *$AlCl_3$–BMIC* (1-Butyl-3-methylimidazolium chloride) melts showed marked improvement over the *$AlCl_3$-EMIC* melts. Aluminum deposits of thickness >0.2 mm were obtained without adding any co-solvent. These melts were also used for the electrorefining of other aluminum alloys such as A356 [17] and Al-MMC [18]. In the present investigation, *$AlCl_3$-BMIC* melts were explored further to determine the influence of various experimental parameters on the aluminum electrorefining process.

2. Experimental

The experimental setup for the electrorefining of aluminum consisted of a 50 ml Pyrex® beaker fitted with a Teflon cap. Schematic diagram of the experimental setup is shown in Fig. 1. Impure aluminum plate, copper/aluminum plate, and pure aluminum wire were used as the anode, cathode and reference electrode respectively. The reference electrode was used to measure the electrode potentials of both anode and cathode individually, using a multimeter (Keithley Instruments Inc®). A constant potential was applied across the electrodes using a Kepco® power source. The experimental setup had provisions for introducing a thermometer and inert gas into the electrolytic cell. Since the electrolyte is moisture sensitive, an inert gas (argon/nitrogen) was introduced into the cell at a flow rate of 50 ml/min to maintain an inert atmosphere above the electrolyte throughout the experiment. The electrolyte was stirred at a constant speed using a magnetic stirrer and the temperature of the electrolyte was controlled by a hot plate (Cole Parmer Vela®). All the experiments were carried out under a vacuum hood.

The electrolyte was prepared by slowly mixing the precisely measured quantities of *$AlCl_3$* and *BMIC* in a dry 50 ml beaker. Since the mixing process was exothermic, *$AlCl_3$* was introduced in small amounts into the beaker containing *BMIC*. Melts formed by rapid combination of the components often have a dark brown color. The melt was then cooled to a predetermined experimental temperature before starting the electrolysis. Careful weighing of the components can yield melts of exact composition with desired physical properties. Excess of *$AlCl_3$* was added to yield acidic melts. Aluminum chloride anhydrous (99.985 %) obtained from Alfa Aesar® was used without further purification. Mixing and weighing of the components were done in a controlled atmosphere glove box filled with argon and the electrolyte was then transferred to the vacuum hood, where the electrolysis was performed.

Deposits obtained on the copper sheet were mechanically separated from the

substrate and powdered for X-ray diffraction studies. X-ray diffraction (XRD) studies were performed on a Rigaku® D/Max-2BX horizontal X-ray diffractometer system, which uses monochromatic Cu-K_α radiation at 50 kV, 200 mA. Compositional analysis of the anodes and deposits were performed using a Philips® PW2400 X-ray fluorescence spectrometer system (XRF).

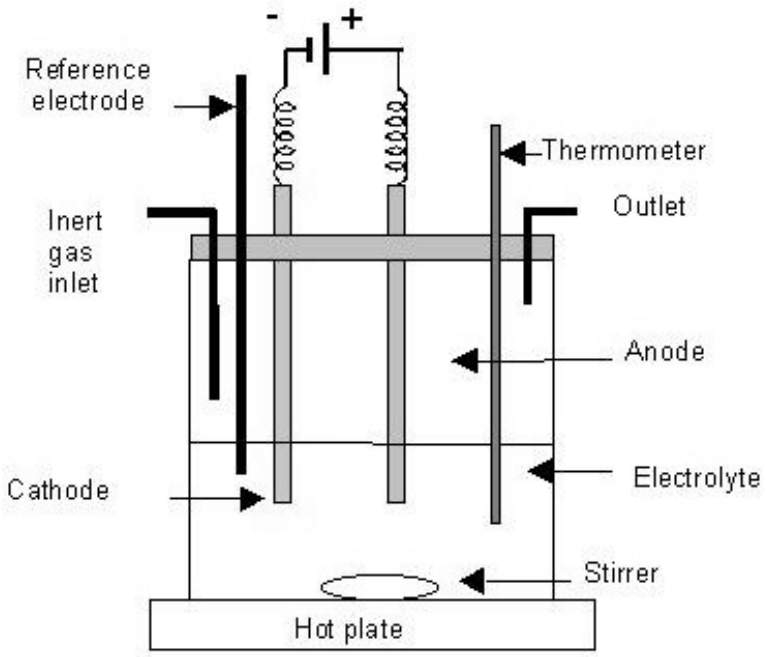

Figure 1. Schematic diagram of the electrolysis experimental setup.

3. Results and discussion

3.1. Electrorefining of aluminum

In the electrorefining process, the impure aluminum alloy (A360) is used as the anode and it is electrorefined in an ionic liquid prepared from $AlCl_3$ and *BMIC*. These melts exhibit Lewis acid-base properties, which vary with the molar ratio of $AlCl_3$:*BMIC* in the melt. Lewis acid is an electron pair acceptor and Lewis base is an electron pair donor. The heptachloroaluminate ion ($Al_2Cl_7^-$) is a strong Lewis acid, while chloride ion is the conjugate Lewis base. Melts with the molar ratio of $AlCl_3$:*BMIC*<1.0 are referred to as

basic melts, and they consist of R^+, Cl^- and $AlCl_2^-$ ions, the exact amounts of which depend on the stoichiometry of the components $AlCl_3$ and $BMIC$ [19]. Melts with the molar ratio of $AlCl_3$:$BMIC$>1.0 are acidic and they are composed of R^+, $AlCl_4^-$ and $Al_2Cl_4^-$ ions.

Aluminum deposition, which proceeds by the reduction of $Al_2Cl_7^-$ ions in the melt, can be explained by the following mechanism. The $AlCl_4^-$ ions present in the melt react with the anode metal to dissolve aluminum and produce $Al_2Cl_7^-$ ions as shown by the anodic reaction (1):

$$Al_{(anode)} + 7AlCl_4^- \leftrightarrow 4Al_2Cl_7^- + 3e^- \quad (1)$$

The dissolved aluminum in the form of $Al_2Cl_7^-$ ions traverses to the cathode either by diffusion or by convection and gets discharged. The cathodic reaction, which leads to the formation of the aluminum deposit, is given by the cathodic reaction (2):

$$4Al_2Cl_7^- + 3e^- \leftrightarrow Al_{(cathode)} + 7AlCl_4^- \quad (2)$$

Aluminum deposition takes place in melts containing excess of $Al_2Cl_7^-$ ions, i.e. in acidic melts. However, in basic melts the concentration of $Al_2Cl_7^-$ ions is extremely small and the dominant chloroaluminate anion, $AlCl_4^-$ is not reducible within the electrochemical window of the melt [13]. Hence, aluminum deposition in acidic melts only was investigated in this study.

In general, electrode reaction rate is governed by the rates of the processes such as electron transfer at the electrode surface, mass transfer of electroactive species from the bulk to the electrode surface, chemical reactions preceding or following the electron transfer, and other surface reactions, such as adsorption, desorption, or crystallization. A steady state current is obtained when the rates of all the above processes are comparable. The electrode reaction rate is monitored by measuring the current at the electrode. The value of this current is limited by the inherent sluggishness of one or more reactions called rate-determining steps. Each of these rate-determining processes can be studied by eliminating the other processes. The mass transfer limitations of the above reactions were eliminated by stirring the electrolyte at a constant speed throughout the experiment. The rate of electrode reactions was studied by varying the parameters such as applied voltage, concentration of electrolyte, and temperature that affect the electrodeposition process.

Electrorefining was performed in the electrolytic cell shown in Fig. 1. A constant voltage was applied across the electrodes. The current output was noted at regularly intervals and it was converted to current density by dividing the current by the cross sectional area of the electrode immersed in the electrolyte. The reported current densities are based on the cathode area measured after the electrodeposition. The optical micrograph of the cross-sectional view of aluminum deposited on copper cathode is shown in Fig.2(a) and the electrodes after electrorefining are shown in Fig. 2(b). The deposit thickness varied from 0.2–0.6 mm for planar deposits and from 0.4–0.9 mm for

dendritic deposits. The gray shiny portion on copper electrode is the deposited aluminum and the black colored portion on the anode is the electrorefined portion. The impurities either remain on the anode or settle at the bottom of the cell as anode sludge. The composition of the aluminum anode obtained by spectrometer analysis is shown in Table 1. After the electrolysis, the deposit was cleaned with acetone and water to remove any organic impurities present on the electrode. The electrolysis was performed for 2 hours.

Table 1. Emission spectrometer analysis of the aluminum alloy

Element	Wt. %
Al	79.77
Si	11.62
Fe	0.76
Mn	0.19
Mg	0.06
Cu	5.00
Ti	0.05
Cr	0.05
Ni	0.08
Zn	2.32
Pb	0.07

The amount of metal deposited was determined by the weight change (ΔW) observed in the cathode before and after electrolysis. The theoretical amount of metal that can be deposited for the quantity of electricity passed during the experiment was determined using the Faraday`s law:

$$W_m = \frac{I \times t \times A_m}{n \times F} \tag{3}$$

where W_m is the theoretical amount of metal deposited, the term $I \times t$ (current × time) is the quantity of electricity supplied, n is the number of electrons transferred in the elementary act of the electrode reaction, A_m is the atomic weight of the metal and F is the Faraday constant (96485 Coulombs). Current efficiency (η_{eff}), which is defined as the ratio of the actual amount of metal deposited to that expected theoretically [20], was calculated by equation (4):

$$\eta_{eff} = \frac{\text{Actual amount of metal deposited } (\Delta W)}{\text{Theoretical amount of metal deposited } (W_m)} \tag{4}$$

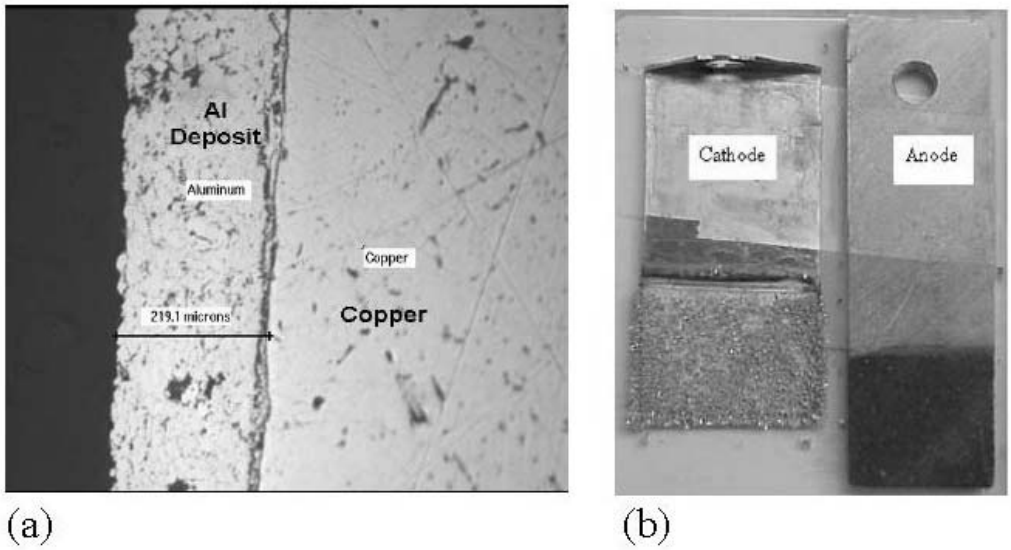

Figure 2. (a) Optical micrograph of aluminum deposited on copper cathode, (b) electrodes after electrorefining.

During electrolysis the cathodic current increased with time. Figure 3 shows the variation of the current density as a function of time for the A360 alloy at concentration ratio of the electrolyte (CR) of 1.5 and temperature 100 °C for different applied potentials. Three distinct characteristic segments can be seen from the plots. In the initial segment (region A), the current density increases rapidly for a short time followed by a steady state increase in the transitional phase (region B), and finally attains a saturation limit in region C. The rapid increase in the current density in region A is due to activation polarization at the cathode. This is confirmed by plotting the cathodic potentials versus logarithm of cathodic current densities in this region as shown in Fig. 4. A linear relation is indicative of activation polarization [21].

In the transitional phase, the current density increases steadily because both activation and concentration polarizations take place. Concentration polarization starts in this region because the concentration of the electroactive species in the cathodic film decreases with time. Thus, the electroactive species has to diffuse through the electrolyte towards the cathode for further deposition to take place. After the transitional phase the current density reaches a limiting value, i.e., a steady state, when concentration polarization alone prevails. The pattern mentioned above is observed at all the voltages as can be seen in Fig. 3.

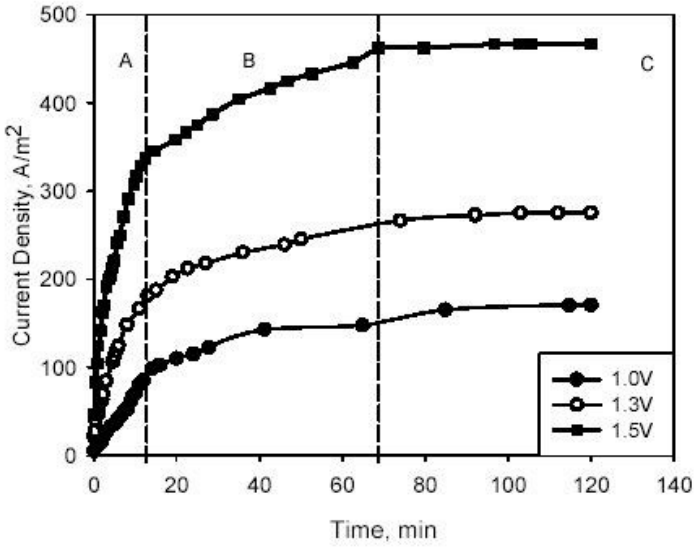

Figure 3. Variation of current density with time at different applied voltages. CR=1.5, temperature=100 ºC for A360 alloy.

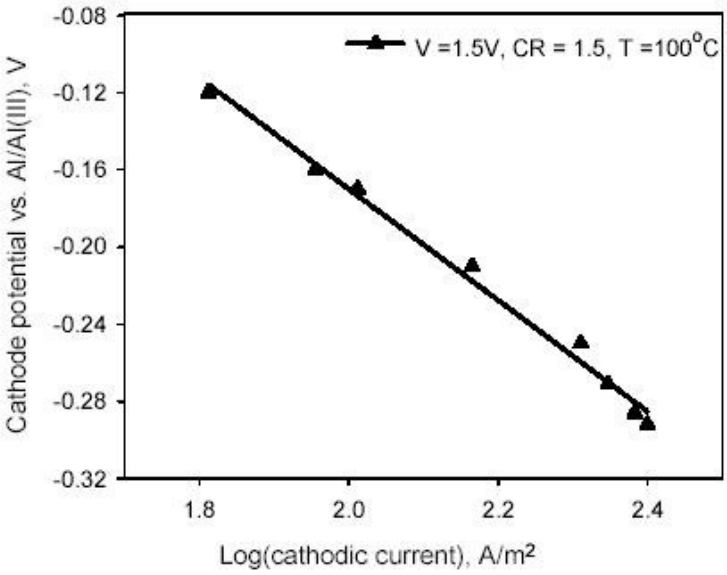

Figure 4. Cathodic polarization curve for aluminum deposition at 1.5 V, CR=1.5 and temperature=100 °C for A360 alloy.

3.2. Effect of cell voltage

The effect of cell voltage on current density and current efficiency of the electrorefining process was studied in the range of 1.0–1.6 V at a constant temperature of 100 °C and a concentration ratio of the electrolyte ($AlCl_3/BMIC$) CR=1.5. Fig. 5 shows the variation of current density and cathodic current efficiency with cell voltage. It can be seen that current density increases with increase in voltage. This increase in current density with voltage is due to the polarization. Moreover, with the increase in voltage the rate of discharge (reduction) at the cathode increases and, as a result, current density also increases.

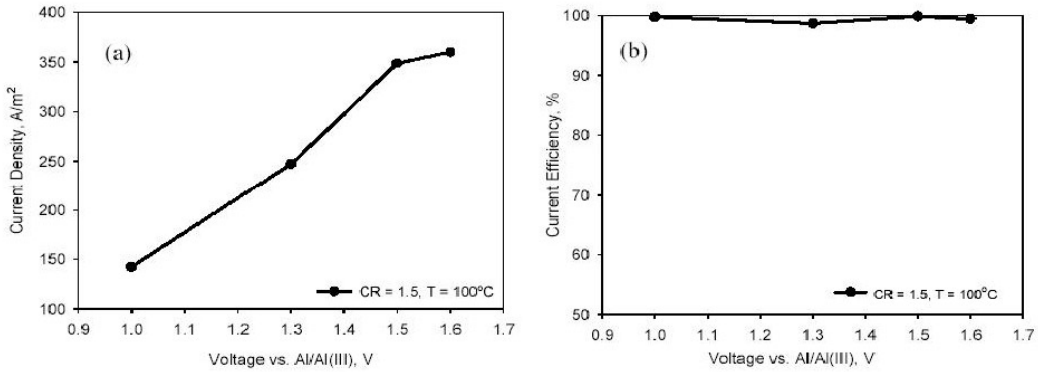

Figure 5. (a) Variation of current density and (b) variation of current efficiency with cell voltage for A360 alloy at CR=1.5 and temperature=100 °C.

Figure 5(b) shows the variation of current efficiency as a function of applied cell voltage for the A360 alloy at a concentration ratio of 1.5 and temperature 100 °C. It can be seen that cathodic current efficiency is well above 98 % at all the voltages. High current efficiencies indicate that there are no reactions taking place other than the deposition of aluminum on the cathode.

3.3. Effect of electrolyte composition

The composition of $AlCl_3$ in the electrolyte plays an important role in the electrorefining process as it determines properties of the electrolyte. Fig.6(a) shows the variation in current density as a function of concentration ratio ($AlCl_3/BMIC$) of the electrolyte at two different applied cell voltages (1.3 and 1.6 V) and temperature 100 °C. No marked difference in current density was observed except at CR=1.6, where a slightly higher current density is observed for both the cell voltages shown in Fig.6(a). A small decrease

in current density at higher concentration ratios may be due to the change in physical properties of the melt. The density of the $AlCl_3$-*BMIC* melts increases with increase in the concentration of $AlCl_3$ in the electrolyte [22]. The increase in density of the melt decreases the mobility of reducible ions ($Al_2Cl_7^-$) towards the cathode. This in turn causes the depletion of electrolyte in the vicinity of the cathode and, as a consequence, current density decreases. Fig.6(b) shows the influence of concentration ratio of the electrolyte on cathodic current efficiency at two different applied cell voltages (1.3 and 1.6V) and a temperature of 100 °C. It can be seen that cathodic current efficiency increases with increase in the concentration ratio from CR=1.5 to CR=1.6 after which it remains constant.

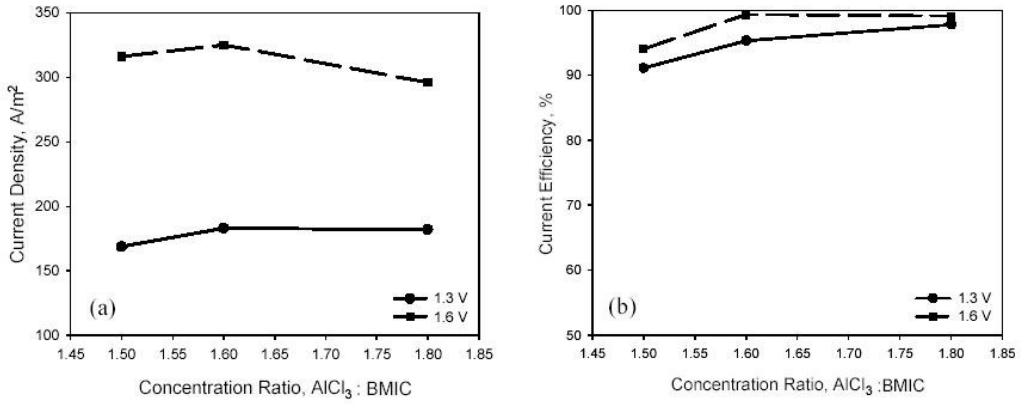

Figure 6. Effect of the concentration ratio of electrolyte on (a) current density and (b) current efficiency for A360 alloy at 100 °C and two different cell voltages.

3.4. Effect of temperature

Electrorefining experiments were performed at different temperatures ranging from 75 to 125 °C. Fig.7(a) shows the variation in current density as a function of temperature at different applied cell voltages (1.0, 1.3, and 1.5 V) and a concentration ratio of 1.5. It was observed that current density increases with increase in temperature. This increase is due to increase in diffusion of reducible ions to the cathode at higher temperatures, thus reducing the concentration polarization.

Temperature influences physical properties of the electrolyte, such as viscosity. Viscosity of the melt decreases with increasing the temperature for the range of concen-

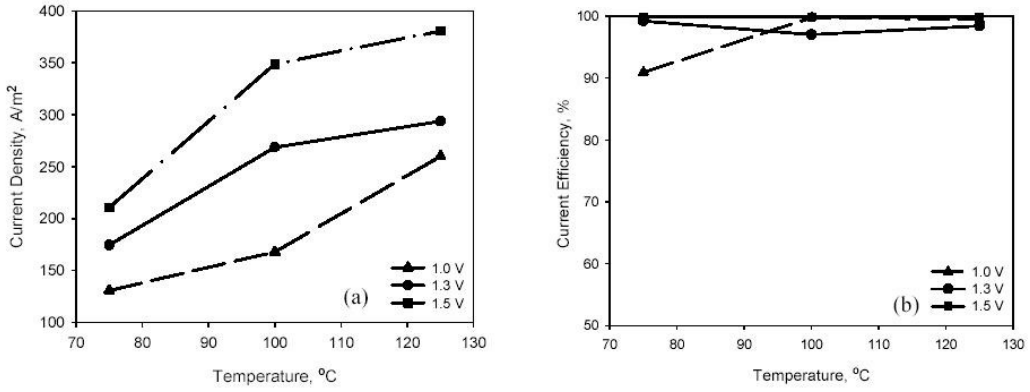

Figure 7. Effect of temperature on (a) current density and (b) current efficiency for A360 alloy at CR=1.5 and different cell voltages.

trations of $AlCl_3$ in the electrolyte used in this study [22]. The decrease in viscosity increases the mobility of ions in the solution, and hence increases the electrode reaction rates. Fig.7(b) shows the variation in cathodic current efficiency as a function of temperature at different applied cell voltages (1.0, 1.3, and 1.5 V) and a concentration ratio of 1.5. It can be seen that cathodic current efficiency increases with increase in temperature for an applied cell voltage of 1.0 V. However, at cell voltages of 1.3 and 1.5 V higher temperature has negligible effect on cathodic current efficiency within experimental errors. Overall, current efficiency at applied cell voltages of 1.3 and 1.5 V and in the temperature range 75–125 °C was above 98 %. High current efficiencies observed in this study indicate that there were no side reactions during the electrorefining process.

The energy consumption (E) during the electrorefining was determined by Eq.(5) using the current efficiency and the applied cell voltage:

$$E = V \times \left(\frac{Q}{\eta_{\text{eff}}} \right) \tag{5}$$

where V is the applied cell voltage, η_{eff} is current efficiency, and Q is the theoretical charge required for depositing a fixed amount of material according to the Faraday`s law. The energy consumption at 1.0 V vs. *Al/Al(III)* was estimated to be 3.0 kWh/kg–*Al*, depending on the applied cell voltage. As the cell voltage increased, energy consumption also increased giving an optimum value at 1.0 V. Aluminum electrodeposition under these experimental conditions had a deposition rate of about 0.0943 g/cm^2 A hr.

The XRD patterns of impure A360 alloy and aluminum deposit are shown in Figs. 8(a) and 8(b), respectively. The XRD analysis for the deposited aluminum shows diffraction peaks of aluminum alone indicating that aluminum deposits were of high

purity. The composition of the electrodeposited aluminum was analyzed using the X-ray fluorescence technique and it is shown in Table 2.

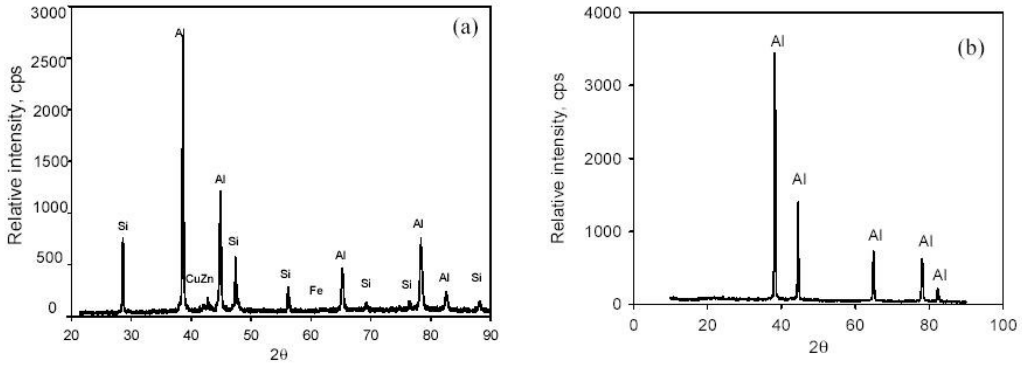

Figure 8. X-ray diffraction pattern for (a) aluminum A360 alloy and (b) aluminum deposited on copper substrate.

Table 2. Composition of the deposited aluminum

Elements	Composition (wt. %)
Al	99.89
Si	0.00
Fe	0.03
Cu	0.03
Mn	0.00
Mg	0.00
Cr	0.00
Ni	0.01
Zn	0.03
Pb	0.00

3.5. Morphology of Al deposits

Aluminum deposited on copper cathode was characterized for morphology by scanning electron microscopy (SEM). It was observed that aluminum chloride content in the melt and the applied cell voltage have significant influence on the morphology of

aluminum deposits. The individual influence of these two parameters on the morphology of aluminum deposits is discussed in the following sections. It was reported that aluminum electrodeposition in these melts is associated with a nucleation process [23]. In fact, large overpotentials were required in order to initiate the deposition of aluminum onto copper electrodes. Moreover, the deposition of aluminum on copper was found to involve instantaneous three-dimensional nucleation with hemispherical diffusion controlled growth of the nuclei [23].

3.5.1. Effect of electrolyte concentration

Fig.9 shows the scanning electron micrographs of aluminum deposited at different concentration ratios (CR=1.0, 1.5 and 1.8) at an applied cell voltage of 1.5 V and 100 ºC. It can be seen that with increase in $AlCl_3$ content in the electrolyte the size of particles increases. Also the clustering of particles can be seen at higher $AlCl_3$ content, i.e., at CR=1.8. At low concentrations of reducible ions, the depletion in diffusion layer at the cathode is considerable. This depletion increases the cathodic polarization and the growth rate of the metal deposit is thus reduced. On increasing the concentration, the cathodic polarization decreases due to the decrease in the thickness of the diffusion layer at the cathode. An increase in the concentration of the ions at the cathode by diffusion favors growth of the existing layer of the deposit resulting in the formation of large grains. Hence, at low concentrations of the electrolyte uniform particle size distribution with a uniform thickness of the deposit was obtained.

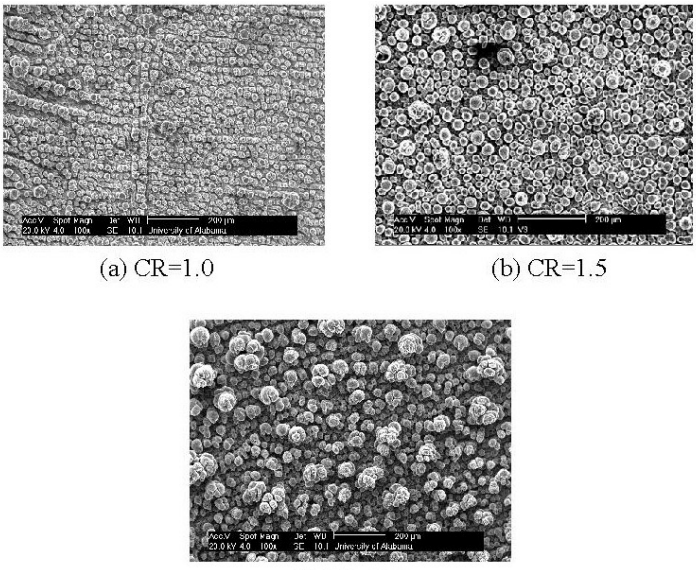

(a) CR=1.0 (b) CR=1.5

(c) CR=1.8

Figure 9. SEM micrographs of aluminum deposited at different concentration ratios of the electrolyte and at a cell voltage of 1.5 V and 100 °C for A360 alloy.

3.5.2. Effect of applied cell voltage

Figure 10 shows the scanning electron micrograph of deposited aluminum at different applied cell voltages (1.0, 1.3 and 1.5 V) at CR=1.5 and 100 °C. At low voltages (1.0, 1.3 V), the clustering or growth of particles can be seen. At low voltages (low current density), the discharge of ions at the cathode is low and so the growth rate of nuclei will be greater than the rate at which new nuclei form; as a result, the deposit becomes coarse [24]. However, as the voltage is increased, the formation of new nuclei is faster than the growth and the deposit becomes fine-grained [25]. This can be seen from Fig. 10 at V=1.5, where fine grains with particle size ranging from 30–40 μm are obtained. Therefore higher applied cell voltages produce a uniform particle size distribution and uniform thickness of the deposit.

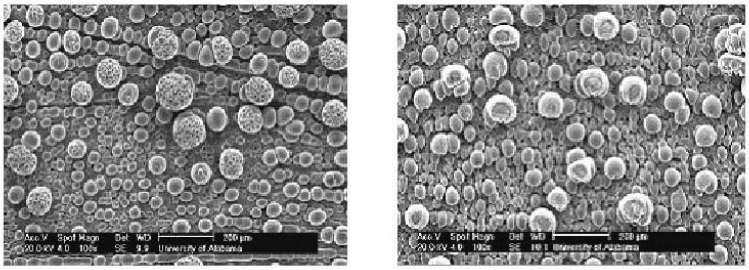

(a) V=1.0 V (b) V=1.3 V

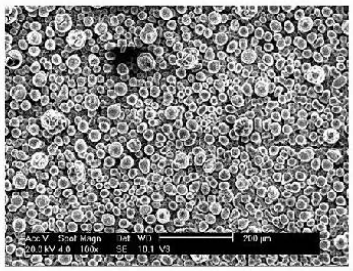

(c) V=1.5 V

Figure 10. The microstructure of aluminum deposited at different voltages mentioned above and at CR=1.5 and 100 °C for A360 alloy.

Hence, it can be seen that at low concentration ratios (CR) of the electrolyte and high cell voltages applied a deposit having uniform thickness with a uniform particle size distribution can be obtained.

4. Conclusions

Aluminum alloy (A360) was electrorefined in an acidic mixture of anhydrous aluminum chloride and 1-Butyl-3-methylimidazolium chloride. High purity aluminum (99.89 %) was obtained in the present study, indicating that the electrorefining of aluminum in ionic liquids yields aluminum of high purity. High voltages and temperatures lead to higher current densities and current efficiencies, whereas higher compositions of $AlCl_3$ in the electrolyte result in lower current densities but higher current efficiencies. Low content of aluminum chloride in the melt and high voltages gave a uniform particle size distribution in the aluminum deposits. This process has the advantage of low energy consumption of about 3.0 kWh/kg–*Al*, as compared to 17–18 kWh/kg-*Al* for the existing industrial refining process.

Acknowledgements

The authors would like to thank the financial support of this research from the US Department of Energy (DOE) under Award number DE-FC07-02ID14397, National Science Foundation (NSF) under the grant number NSF-EPS-9977239 and The University of Alabama at Tuscaloosa (UA). We also thank Mr. R. Nagireddy for helping in preparing the ionic liquids used in the present study.

References

1. Metals Handbook, J. R. Davis (Editor), ASM International, 1998, p. 417-499.
2. L. Guohua, L. Dianfeng, and W. Qingna, Study of the Cathodic Process in the Three-layer Electrolytic Refining of Aluminum, (Light Metals 1997, TMS, Warrendale, PA, 1997), p. 417-420.
3. M. Kondo, H. Maeda, and M. Mizuguchi, Journal of Metals, 42 (1999) 36.
4. R. Bunsen, Poggendorf' Ann., 97 (1854) 648.
5. D.B. Keyes and S. Swann, U.S. Patent. 1,939,397, December 12, (1933).
6. K.R. Seddon, Journal of Chemical Technology and Biotechnology, 68 (1997) 351.
7. F.H. Hurley, Electrodeposition of Aluminum, U.S. Patent. 2,446,331, August 3, (1948).
8. T.P. Wier, Jr., Electrodeposition of Aluminum, U.S. Patent. 2,446,350, August 3, (1948).
9. G.A. Capuano and W.G. Davenport, J. Electrochem. Soc., 118 (1971) 1688.
10. E. Peled and E. Gileadi, J. Electrochem. Soc., 123 (1976) 15.
11. B.J. Welch and R.A. Osteryoung, J. Electroanal. Chem., 118 (1981) 455.
12. J.S. Wilkes, J.A. Levisky, and C.L. Hussey, Inorg. Chem., 21 (1982) 1263.
13. R.T. Carlin, W. Crawford and M. Bersch, J. Electrochem. Soc., 139 (1992) 2720.

14. C.L. Hussey, G.R. Stafford, W.R. Pitner, Q. Liao and G. Stewart, J. Electrochem. Soc., 144 (1997) 936.
15. B. Wu, R.G. Reddy, and R.D. Rogers, Proc. Fourth International Symposium on Recycling of Metals and Engineered Materials, TMS, 2000, p. 845-856.
16. B. Wu, R.G. Reddy, and R.D. Rogers, Aluminum Reduction via Near Room Temperature Electrolysis in Ionic Liquids, (Light Metals 2001, TMS, 2001), p. 237-243.
17. V. Kamavaram and R.G. Reddy, Recycling of Aluminum based Materials in Ionic Liquids, (Recycling and Waste Treatment in Mineral and Metal Processing, TMS, 2002), p. 517-526.
18. V. Kamavaram and R.G. Reddy, Proc. Ninth International Conference on Composite Engineering, ICCE/9, 2002, p. 359.
19. Z.J. Karpinski and R.A. Osteryoung, Inorg. Chem., 23 (1984) 1491.
20. R. Sharan and S. Narain, An Introduction to Electrometallurgy, Standard Publishers, New Delhi, 1969, p. 47.
21. A.J. Bard and L.R. Faulkner, Electrochemical Methods, John Wiley, New York, 2000, p. 87.
22. V. Kamvaram and R. G. Reddy, Physical and Thermal Properties of Ionic Liquids Used in Aluminum Electrorefining at Low Temperatures, (Aluminum 2003, TMS, 2003)(in press).
23. V. Kamavaram and R.G. Reddy, Electrochemical Studies of Aluminum Deposition in Ionic Liquids at Ambient Temperatures, (Light Metals 2002, TMS, 2002), p. 253-258.
24. S. Glasstone, An Introduction to Electrochemistry, D. Von Nostrand Company, New York, 1942, p. 482.
25. C.C. Yang, Materials Chemistry and Physics, 37 (1994) 355.